www.ietdl.org

Published in IET Image Processing
Received on 22nd October 2012
Revised on 31st January 2013
Accepted on 19th February 2013
doi: 10.1049/iet-ipr.2012.0614

ISSN 1751-9659

Low-bit depth-high-dynamic range image generation by blending differently exposed images

Jae-Il Jung, Yo-Sung Ho

Gwangju Institute of Science and Technology (GIST), 123 Cheomdangwagi-ro, Buk-gu, Gwangju 500-712, Korea
E-mail: jijung@gist.ac.kr

Abstract: Recently, high-dynamic range (HDR) imaging has taken the centre stage because of the drawbacks of low-dynamic range imaging, namely detail losses in under- and over-exposed areas. In this study, the authors propose an algorithm for HDR image generation of a low-bit depth from two differently exposed images. For compatibility with conventional devices, HDR image generations of a large bit depth and bit depth compression are skipped. By using posterior probability-based labelling, luminance adjusting and adaptive blending, the authors directly blend two input images into one while preserving the global intensity order as well as enhancing its dynamic range. From the experiments on various test images, results confirm that the proposed method generates more natural HDR images than other state-of-the-art algorithms regardless of image properties.

1 Introduction

Generally, commercial digital image sensors fail to capture scenes visible to humans. Primarily, this is because of the limited dynamic range of the image sensors; improper camera settings occasionally cause the problem as well. Humans can perceive scene luminance varying from 10^{-3} to 10^5 cd/m^2; however the dynamic range of an ordinary digital image sensor is only about 10^2 cd/m^2 [1]. In order to maximise the use of this limitation, digital cameras allow users to control exposure settings by their preferences. However, this procedure is not suitable when the scene to be captured has a much wider dynamic range than the cover range of the camera.

Various algorithms have been proposed [2–4] for visual quality improvement of such low-dynamic range (LDR) images; yet their performances have shown shortcomings owing to insufficient data in brighter or darker regions. Consequently, high-dynamic range (HDR) imaging has taken centre stage in recent years. Compared with LDR imaging, HDR imaging uses wider dynamic range, larger bit depth and higher fidelity.

Special sensors and computer graphics have been developed to capture HDR images. The most widely used method is weighed summation of multiple LDR images [5–7]. Although the large-bit depth enables containment of elaborate data, it has to be compressed to the general bit depth of LDR images for compatibility with commercial devices. This process is called tone mapping.

In other words, we have to synthesise an HDR image of a high-bit depth and compress it through tone mapping to acquire the low-bit depth version; this is an inefficient process. In this paper, we propose an image blending algorithm that directly blends an HDR image of low-bit depth from two differently exposed images. The main contribution of our work is avoiding unnatural colour changes during contrast enhancement and preserving relative radiance of scenes. In addition, in order to enhance contrast and generate sharp edges we calculate likelihood probabilities of all pixels in both images. Afterward, they are globally optimised with consideration of prior probabilities. Lastly, two images are adaptively blended into one. The proposed method directly generates low-bit depth HDR images, which are visually more natural compared with results by conventional works.

The remainder of this paper is organised as follows: Section 2 provides a comprehensive review of conventional techniques. In Section 3, we introduce the proposed algorithm in detail. The effectiveness of the system is compared with other state-of-the-art algorithms in Section 4. Finally, this paper concludes in Section 5.

2 Image quality enhancement

Various algorithms have been developed to enhance the visual quality of images. This section provides a brief coverage of some of the techniques that share similar features with the proposed algorithm.

In the earlier era, image enhancement techniques for LDR images such as histogram stretching and equalisation were developed. These methods enhance contrast by modifying pixel values in rarely used histogram bins. Despite their simplicity and reliability, excessive colour changes occasionally occur.

To encounter this problem, Kim [8] divided the LDR image into two and independently equalised each histogram. This algorithm is able to enhance image contrast while preserving the mean brightness of images. Later, Menotti *et al.* [9] have extended Kim's method. They decomposed the input image into several sub-images and equalised each sub-histogram. Wang *et al.* [4] have found the flattest target histogram for contrast enhancement subject to the mean brightness. For estimating the flattest histogram with brightness preservation, they used convex optimisation and exacted histogram specification. Im *et al.* [10] have proposed a single image-based HDR image generation algorithm using local histogram stretching. They also adopted edge-preserving spatially adaptive denoising algorithm to suppress amplified noise during local histogram stretching.

Recently, Tsai and Yeh [11] have presented a piecewise linear transformation enhancing image contrast to avoid non-linear approaches of the algorithms based on histograms. Jha *et al.* [3] have proposed a stochastic resonance-based approach to enhance very low contrast images with reducing artefacts and colour loss.

The above mentioned algorithms successively improve contrast of LDR images, but their performances are limited when input images have under- and over-exposed regions. Therefore HDR imaging technologies have been actively researched as an alternative. The main challenge of HDR image-based approaches is the bit depth compression; the bit depth of HDR images should be effectively compressed to the bit depth compatible with conventional electronic devices.

In literature, tone mapping algorithms are divided into global and local approaches. Global approaches adopt a spatially invariant mapping curve to accelerate process and generate natural results. Tumblin and Rushmeier [12] have proposed a sensation-preserving display converter based on observer models. They defined the relation between display luminance and real-world luminance. Larson *et al.* [13] have developed a histogram adjustment technique considering contrast and colour sensitivities to match viewing experience.

To emphasise local contrast, several tone mapping algorithms have exploited local approaches as the human visual system operates. Such approaches use spatially variant mapping curves by referring to neighbouring pixels. Drago *et al.* [14] have developed logarithmic compression imitating the human response to light, proposing improved gamma correction for contrast enhancement in dark regions. Fattal *et al.* [15] have manipulated a gradient field and produced LDR images by soling a Poisson equation.

Recently, various tone mapping algorithms have been proposed considering the human visual system to reduce unnatural artefacts. Reinhard and Devlin [16] have proposed dynamic range reduction with consideration of the adaptation processes which occur in the human visual system. Physiological evidence suggests that adaptation already occurs in photoreceptors, leading to a straightforward model that can be easily adapted for tone reproduction.

Mantiuk *et al.* [17] have suggested a tone mapping algorithm that minimises visible contrast distortions. This algorithm covers various output devices such as e-paper to HDR displays. The distortions are also predicted by the model of the human visual system. Krawczyk *et al.* [18] have proposed a tone reproduction method based on the theory of lightness perception. This method is inspired by the anchoring theory related to lightness constancy and its spectacular failure.

Some researchers have proposed image fusing algorithms [19–22]. Since these algorithms insufficiently consider relative radiance of scenes and only fuse high contrast regions, they provide unnatural output images because of the wrong intensity order. In addition, these algorithms require multiple images (generally more than two), which can induce the ghost artefact, which means object boundaries are misaligned in the fused image.

Further, in the current trend, HDR imaging has been extended to three-dimensional image processing. Ning *et al.* [23] have proposed HDR stereo image generation algorithm from differently exposed stereoscopic images. They estimate disparities between pairs and mix two images. Sharma *et al.* [24] have developed multi-view multi-exposure image synthesis and HDR stereo reconstruction.

3 Posterior probability-based image blending

The existing approaches only focus on local contrast enhancement since they can induce excessive colours, halo artefacts and intensity order inversion. In this paper, we propose an image blending algorithm of two differently exposed images, which naturally enhances local details and preserves the intensity order. Although more than two images have been used for HDR imaging, capturing multiple images of dynamic scenes is challenging. Motions in scenes induce the ghost effect, meaning object boundaries are misaligned in the fused image. Thus, we use two images to effectively minimise this artefact.

Unlike conventional HDR tone mapping algorithms, an HDR image of a high-bit depth is not generated during the process. To this end, the proposed algorithm exploits several steps as shown in Fig. 1. Since we adjust luminance components and map chrominance components during the process, we adopt the YUV colour domain. This allows to independently adjust luminance components and to calculate magnitude of chrominance components.

The most important tasks are identifying well-exposed textures from two inputs and blending them naturally. Finding well exposed region from two images is regarded as the labelling problem for assigning a label s to each pixel, where $s = \{L, H\}$. By applying the Bayes rule, the posterior probability of S can be expressed as

$$P(S|I_L,\ I_H) = \frac{P(I_L,\ I_H|S)P(S)}{P(I_L,\ I_H)} \tag{1}$$

where $P(S)$ is the prior probability of the labelling set S. $P(I_L, I_H/S)$ is the conditional probability density function of I_L and I_H given S. $P(I_L, I_H)$ is ignorable since unknowns are not contained; this is a constant when I_L and I_H are given. Therefore the maximum a posterior is equivalently found by

$$\arg\max_S \{P(I_L,\ I_H|S)P(S)\} \tag{2}$$

Since the model of S is designed via the Markov random field, the posterior probability $P(S|I_L, I_H)$ can be characterised by the Gibbs distribution [25], which is expressed as

$$\begin{aligned} &P(S|I_L,\ I_H) = Z^{-1} \times \exp\left(-\frac{1}{T}E(S|I_L,\ I_H)\right) \\ &\text{where } Z = \sum_S \exp\left(-\frac{1}{T}E(S|I_L,\ I_H)\right) \end{aligned} \tag{3}$$

where Z is a normalising constant called the partition

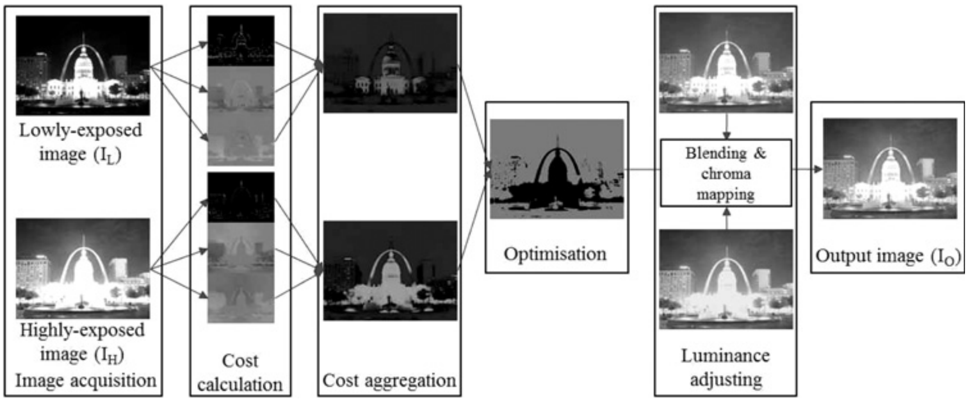

Fig. 1 *Schematic of the proposed algorithm*

function, and T is a constant representing the temperature. $E(S|I_L, I_H)$ is the energy function. Therefore (2) is replaced by the minimisation problem of the energy function E as

$$\arg\min_S\{E(I_L,\ I_H|S) + E(S)\} \tag{4}$$

3.1 Cost calculation

The likelihood energy $E(I_L, I_H|S)$ measures the disagreement between estimated and observed data. The proposed algorithm considers not only gradient values but also magnitude values of chrominance components as observed data. In general, well-exposed regions carry larger gradient values and more vivid colours than over- or under-exposed regions. Based on such characteristics, the sum of cost values is used for the likelihood energy as

$$E(I_L,\ I_H|S) = \sum_{x,y} \text{cost}_{S(x,y)}(x,\ y) \tag{5}$$

The cost value is defined as

$$\begin{aligned}\text{cost}_s(x,\ y) = 2^k - \text{grad}_s(x,\ y) \\ + \lambda_C\{2^{k-1} - \max(|U_s(x,\ y) - 2^{k-1}|, \\ |V_s(x,\ y) - 2^{k-1}|)\}\end{aligned} \tag{6}$$

where k is a bit depth for grey representation and the subscription $_S$ is the label. The second term penalises the cost for small chrominance values, U or V. λ_c is a weighting constant grad returns the largest gradient value among four-connected neighbours in the luminance domain, Y, as

$$\begin{aligned}\text{grad}_S(x,\ y) = \max(&|Y_S(x,\ y) - Y_S(x+1,\ y)|, \\ &|Y_S(x,\ y) - Y_S(x-1,\ y)|, \\ &|Y_S(x,\ y) - Y_S(x,\ y+1)|, \\ &|Y_S(x,\ y) - Y_S(x+1,\ y-1)|)\end{aligned} \tag{7}$$

These cost values for I_H and I_L are normalised and shown in Fig. 2*a*. Since the cost values are calculated pixel-by-pixel, the individual value has low correlation among neighbouring pixels. In addition, cost values of homogeneous regions do not have enough discernment.

3.2 Cost aggregation and optimisation

To enhance the spatial correlation and propagate discernment, cost values are aggregated with consideration of their neighbours and corresponding colours. We adopt a joint-bilateral filter (JBF) to the cost maps since the surface of the labelling set is piecewise smooth and the close pixels with similar colours tend to have similar costs. In this paper, JBF used is designed as

$$\text{cost}_s^t(x,\ y) = \frac{\sum_{x'\in Nx}\sum_{y'\in Ny} w_c(x,\ y,\ x',\ y')\text{cost}_s^{t-1}(x',\ y')}{\sum_{x'\in Nx}\sum_{y'\in Ny} w_c(x,\ y,\ x',\ y')} \tag{8}$$

$\Delta c(x, y, x', y')$ is the Euclidean distance between pixels at (x, y) and (x', y') in the colour domain. Similarly, $\Delta g(x, y, x', y')$ is the Euclidean distance in the image domain. t is the iteration number and N represents neighbours in a 10×10 local block. γ_c and γ_g are set to 0.1 and 5 in this system. To prevent undiscerning cost propagation, we add a conditional statement as (9). This constraint excludes costs lower than the current cost from references, preventing undiscerning cost propagation.

We design the prior term in (4) considering the smoothness constraint that neighbourhoods of images present some coherence and do not change abruptly except at boundaries. We characterise the prior model by the multilevel logistic as

$$E(S) = \lambda_p \sum_{x,y} \sum_{x',y'\in N_4} 1 - \delta(S(x,\ y),\ S(x',\ y')) \tag{10}$$

$E(S)$ penalises the labels which have different values than four-connected neighbours, N_4 and λ_p means a weighting factor for the prior energy. When $S(x, y)$ is equal to $S(x', y')$, δ returns one, otherwise returns zero. The posterior probability is optimised via belief propagation to infer

$$\text{where } w_c(x,\ y,\ x',\ y') = \begin{cases} \exp\left(-\left(\dfrac{\Delta c(x,\ y,\ x',\ y')}{\gamma_c} + \dfrac{\Delta g(x,\ y,\ x',\ y')}{\gamma_g}\right)\right) & \text{cost}_s^{t-1}(x,\ y) \le \text{cost}_s^{t-1}(x',\ y') \\ 0 & \text{otherwise}\end{cases} \tag{9}$$

doi: 10.1049/iet-ipr.2012.0614

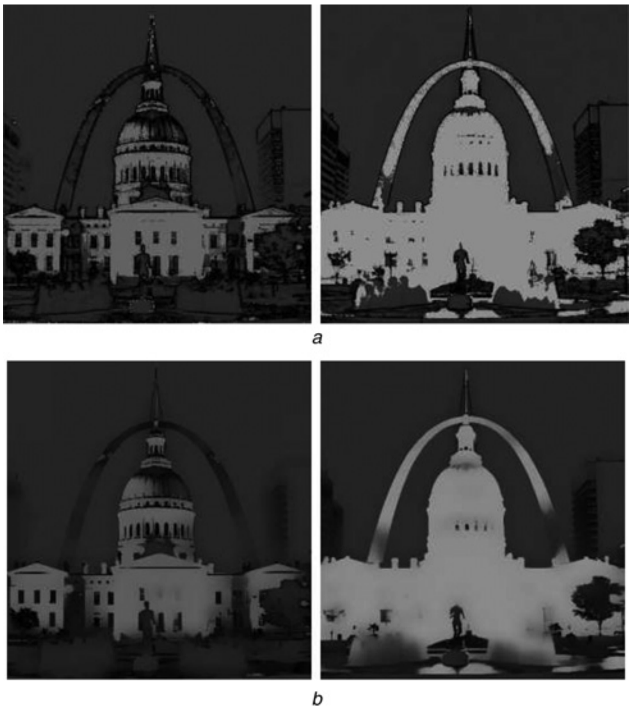

Fig. 2 *Initial cost maps for the likelihood model and refined maps*

a Initial cost maps of I_L and I_H
b Refined cost maps

the optimised S [26]. The final label set S is shown in Fig. 5, and the two input images are selectively blended according to S.

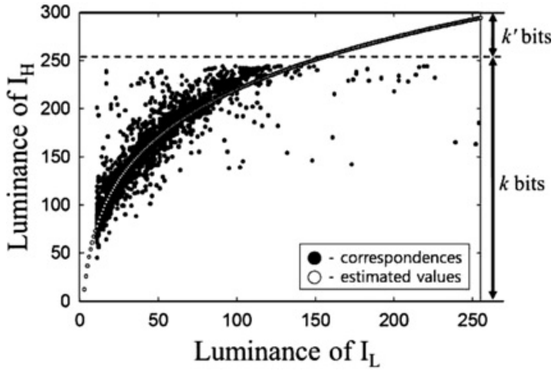

Fig. 3 *Luminance relation between inputs and additional bits k'*

3.3 Luminance adjusting

Although the label set was estimated using various factors, simple copy referring to the label set can cause problems such as grey inversion and boundary mismatch. To solve this problem, we conduct additional steps to match radiance levels of inputs and adaptively blend them.

Although conventional algorithms acquire exposure information from metadata of input images, the proposed algorithm automatically measures it by analysing luminance differences between correspondences. Initially, co-located luminance values are extracted from inputs, which are regarded as correspondences. The correspondences whose luminance values are greater than 0.95×2^k or less than 0.05×2^k are excluded to reduce influence of under- or over-exposed regions.

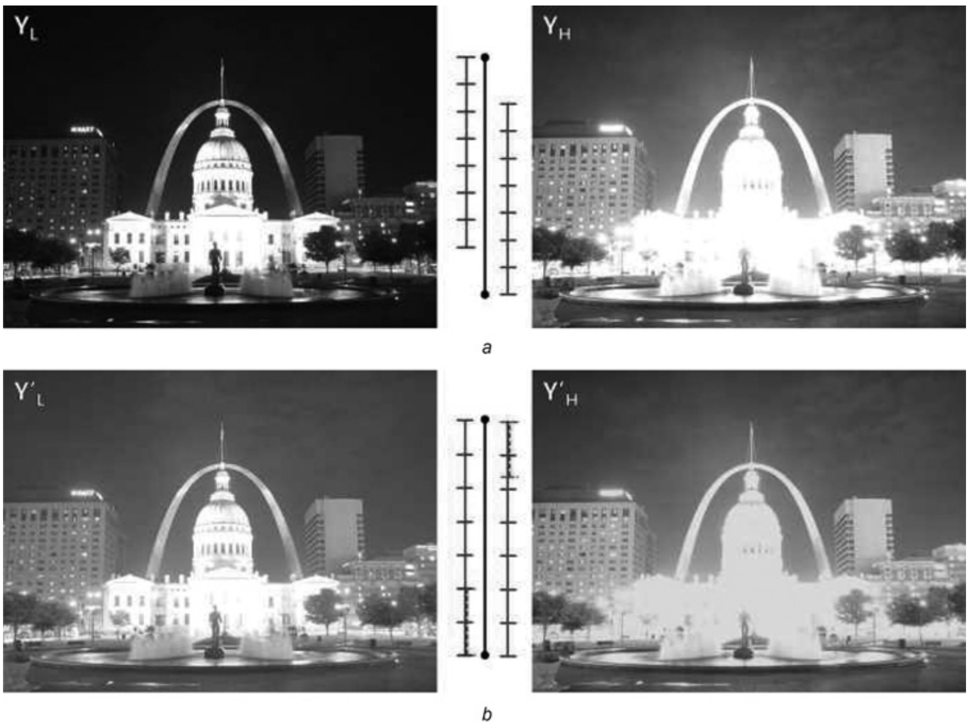

Fig. 4 *Input luminance images, Y_L and Y_H and the adjusted images, Y'_L and Y'_H*

The centre line is the entire dynamic range of the scene, and the two lines with gradations represent the coverage with k bits
The dotted lines mean the unused ranges in (b)
a Initial lumiance images
b Adjusted luminance images

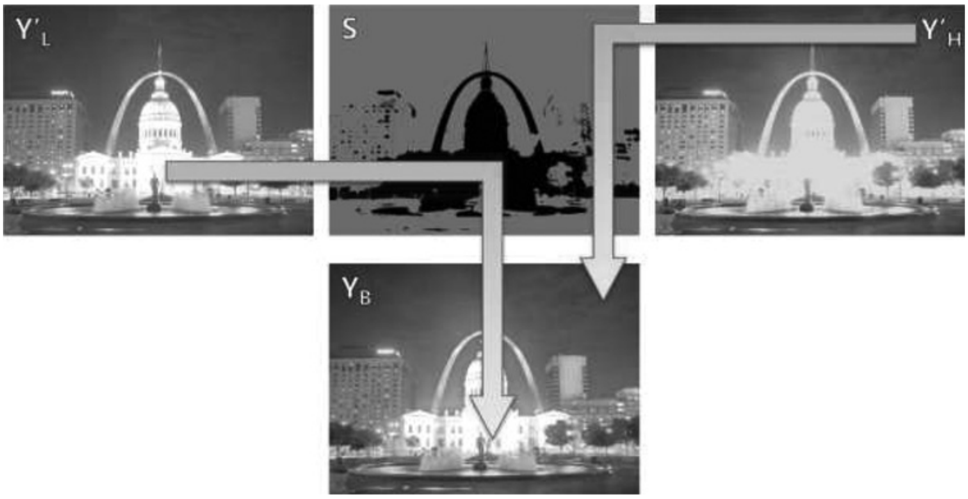

Fig. 5 *Schematic illustration of image blending based on the label set S*

The luminance relation between inputs is defined as (11), considering gain, offset and gamma of capturing conditions

$$\begin{aligned} Y_H &= f_d\left(Y_L,\ \bar{C}\right) \\ &= C_{\text{gain}}\left\{Y_L/\left(2^k-1\right)\right\}^{C_{\text{gamma}}}\times\left(2^k-1\right)+C_{\text{offset}} \end{aligned} \quad (11)$$

where C_{gain}, C_{offset} and C_{gamma} represent coefficients for each camera property and $\bar{C}$ stands for the coefficient vector. Owing to the non-linearity of f_d, we estimate these coefficients via the Levenberg-Marquardt algorithm [27].

Fig. 3 demonstrates the luminance relation between the luminance levels of I_H and I_L. The black and white dots represent the correspondences and estimated values, respectively. Since I_H was captured with high exposure, additional k' bits are required to represent I_L in the same luminance level as

$$k^+ = k + k' \text{ where } k' = \log_2 f\left(2^k,\ \bar{C}\right) - k \quad (12)$$

This process is inefficient since the extended bit depth has to be compressed again for compatibility. Therefore we adjust bit representation of two inputs so that each image covers

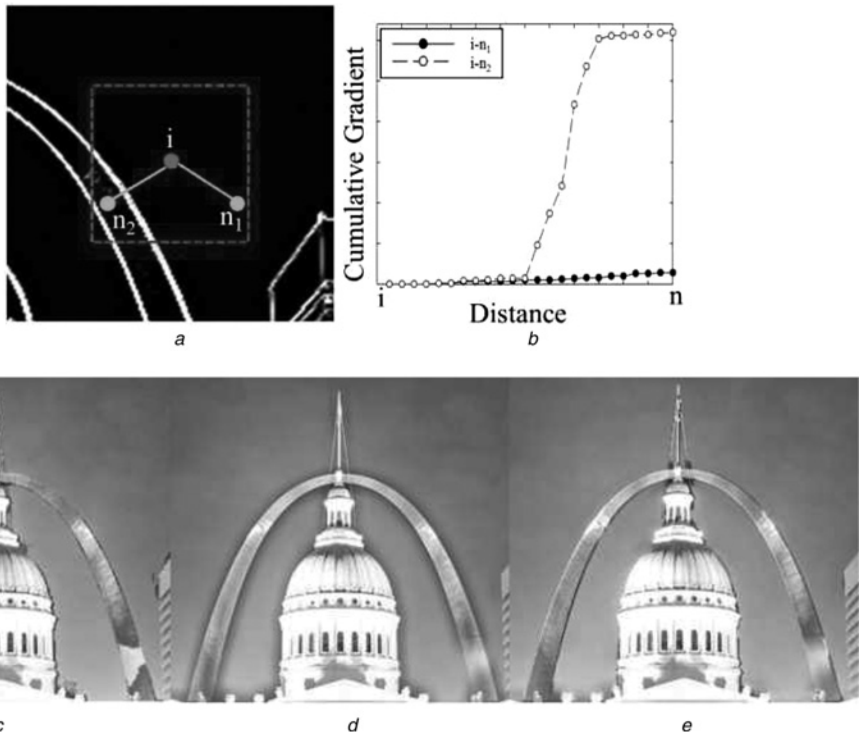

Fig. 6 *Example of CGs and the blending results*

a Current pixel i and its two neighbours, n_1 and n_2
b Cumulative gradients for n_1 and n_2
c Copying method
d Averging method
e Proposed blending method

doi: 10.1049/iet-ipr.2012.0614

the entire dynamic range of the scene with k bits. Fig. 4*a* shows the luminance images of the inputs, the black line is the entire dynamic range of the scene, and the blue lines represent the coverage of the images with k bits. Depending on the exposure settings, the coverage of bits becomes different.

By using (13) derived from (11) and (12), we modify the luminance components of inputs so that each image covers the entire dynamic range of the scene even though some bits are unused

$$\begin{aligned} Y_L'(x, y) &= \text{scaling} \times \left(C_{\text{gain}} \times Y_L(x, y)^{C_{\text{gamma}}} + C_{\text{offset}}\right)^{\text{gamma}} \\ Y_H'(x, y) &= \text{scaling} \times Y_H(x, y)^{\text{gamma}} \\ \text{where scaling} &= 2^k/2^{k+} \end{aligned} \tag{13}$$

In (13), gamma is a parameter for gamma correction, set to 0.8. Fig. 4*b* shows the adjusted results and the red lines represent the unused bits. These unused bits are blending margins and filled during the following blending process.

3.4 Blending and chroma mapping

With the adjusted images, Y'_L and Y'_H and the label set S, we are able to synthesise the blended luminance image Y_B as shown in Fig. 5. The black and grey regions of S are filled with the textures of the Y'_L and Y'_H, respectively.

However, simple copying can induce unnatural boundaries as shown Fig. 6*c*, and averaging of labels over local blocks causes halo artefacts as shown in Fig. 6*d*. Therefore we adopt an adaptive weight for a local block to naturally blend two luminance components of Y'_L and Y'_H as

$$Y_O(x, y) = \frac{\sum_{x' \in Nx} \sum_{y' \in Ny} w_b(x, y, x', y') Y_{S(x',y')}(x', y')}{\sum_{x' \in Nx} \sum_{y' \in Ny} w_b(x, y, x', y')} \tag{14}$$

where N means the neighbours in a local block of 10×10. w_b represents the weighting coefficient considering a cumulative gradient (CG) value of the shortest path between (x, y) and (x', y'). CG is the sum of the gradient values over the path. Figs. 6*a* and *b* shows the concept of CG. In Fig. 6*a*, there are the two neighbours, n_1 and n_2, of current pixel i, they have the same length of the shortest paths but different CGs as shown in Fig. 6*b*. With CGs, we allocate greater weighting values to neighbouring labels which might be on the same objects. The weighting value w_b considering CG is calculated as

Table 1 Consumed time

Step	Time, s	Ratio, %
image loading	0.02	0.43
luminance adjusting	0.80	17.13
gradient calculation	0.06	1.28
cost aggregation	2.32	49.68
optimisation	0.43	9.20
blending	0.92	19.70
image saving	0.12	2.57
total	4.67	100

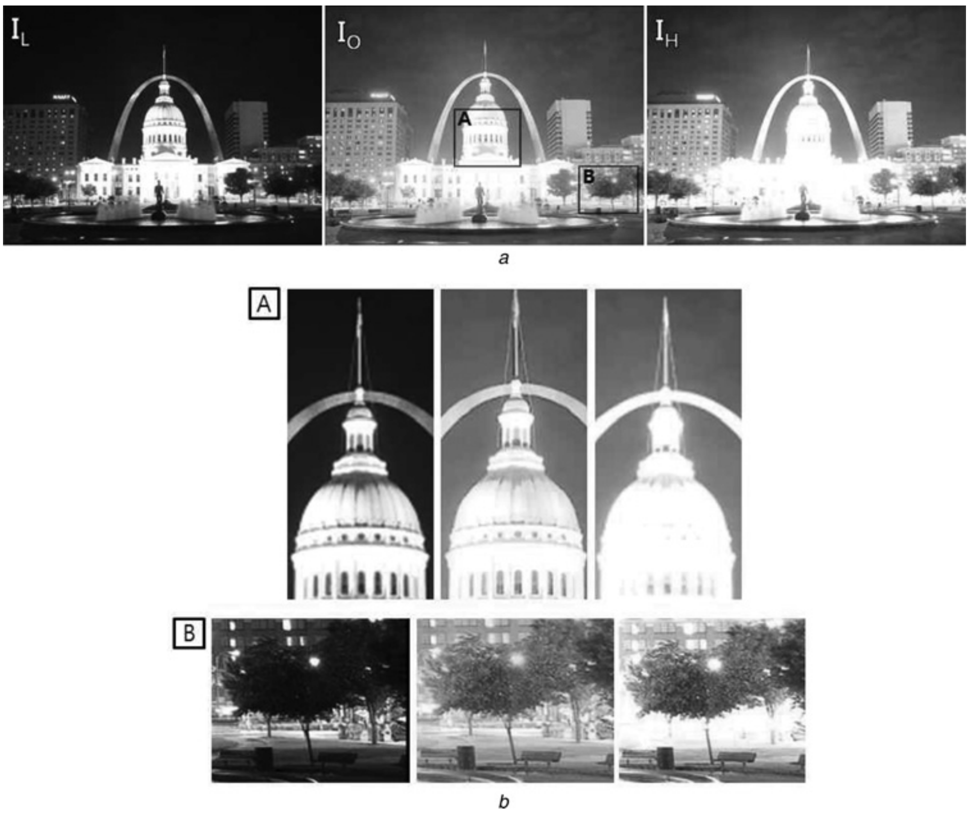

Fig. 7 *Final results of the proposed algorithm and enlarged parts*

a Input image I_o
b Enlarged parts: I_L, I_o and I_H

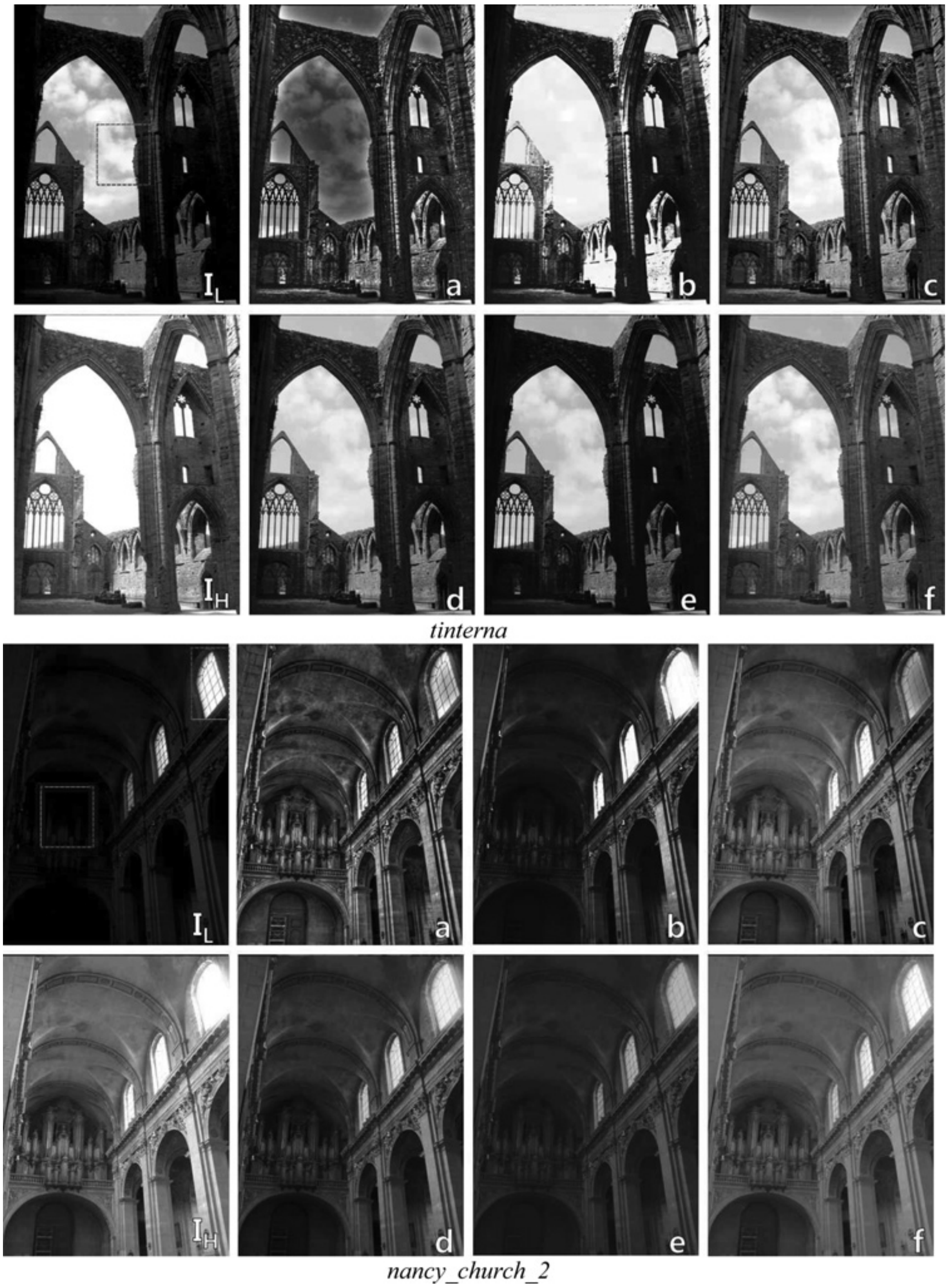

Fig. 8 *Input and result images*
a Fattal
b Krawczyk
c Mertens
d Mantiuk
e Reinhard
f Proposed

$$w_b(x, y, x', y') = \exp\left(-\frac{\mathrm{CG}(x, y, x', y')}{\gamma_{CG}}\right)$$

where $\mathrm{CG}(x, y, x', y')$

$$= \sum_{(x', y') \in \mathrm{path}(x, y - x', y')} \max\{\mathrm{grad}_L(x', y'), \mathrm{grad}_H(x', y')\} \tag{15}$$

where γ_{CG} is set to 10. Fig. 6*e* shows the result of the proposed method. For observation, we did not apply the luminance adjusting step in Figs. 6*c*–*e*. Although copying and averaging methods fail to generate natural boundaries, the proposed method produces clear boundaries and smooth homogenous regions without halos.

Following blending, chroma components are added to Y_{B}. For reconstructing vivid colours, larger chrominance values between the inputs are selected and referred. This process is conducted pixel-by-pixel, and represented as

$$U_O(x, y) = \max\{|U_H(x, y) - 2^{k-1}|, \quad |U_L(x, y) - 2^{k-1}|\}$$
$$V_O(x, y) = \max\{|V_H(x, y) - 2^{k-1}|, \quad |V_L(x, y) - 2^{k-1}|\} \tag{16}$$

doi: 10.1049/iet-ipr.2012.0614

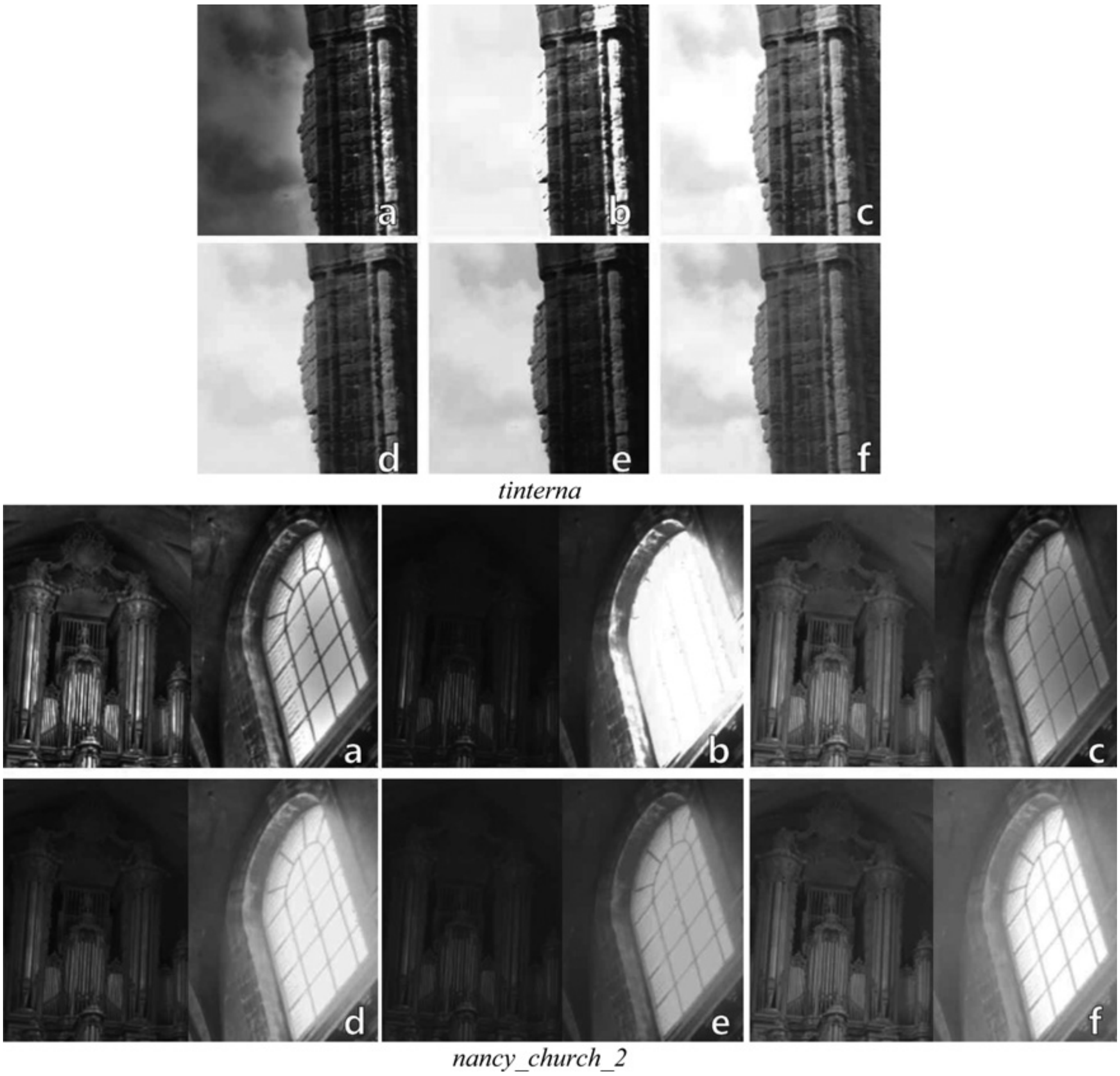

Fig. 9 *Enlarged parts of Fig. 8*

a Fattal
b Krawczyk
c Mertens
d Mantiuk
e Reinhard
f Proposed

4 Experimental results

To evaluate the performance of the proposed algorithm, a series of experiments were conducted on a 3.2 GHz CPU. t, λ_c and λ_p were set to 3, 0.1 and 0.3, respectively. These empirically determined parameters were used for all experiments. Since only two labels exist, image blending of a 800×600 image can be achieved in 4.7 s on average. Table 1 shows the processing times for each step. The cost aggregation using JBF and view blending process is relatively lengthier time than other processes. These steps can be accelerated by simplifying algorithms [28] for some special applications that require little computational time.

Fig. 7*a* shows the I_L, I_H and output image I_O, and Fig. 7*b* exhibits the enlarged parts of A and B. The proposed algorithm successively found well-exposed regions from the input images, and naturally blended these regions into one. Especially in part B, I_O successively reveals the detail of leaves of I_H and the bottom of the building of I_L without unnatural colour changes.

For comparison, additional experiments were carried out with five representative and recent algorithms: (i) Fattal *et al.* [15], (ii) Krawczyk *et al.* [18], (iii) Mertens [20], (iv) Mantiuk *et al.* [17] and (v) Reinhard [16]. After generating HDR images from two input images, we applied each algorithm to the data. We use 20 HDR images downloaded from http://www.pauldebevec.com/Research/HDR/ as test images. Fig. 8 shows the two input images (left column) and each result, and Fig. 9 demonstrates the enlarged textures of the red boxed regions of Fig. 8.

Fattal's and Merten's algorithms display very impressive results, but they create halo artefacts around boundaries between bright and dark regions. Although Krawczyk's algorithm loses bright textures, Mantiuk's and Reinhard's algorithms are not efficient at expressing dark regions. Even though conventional algorithms generate unnatural results as shown in these tests, the proposed algorithm demonstrates satisfactory subjective results and successfully reveals texture details in both bright and dark regions.

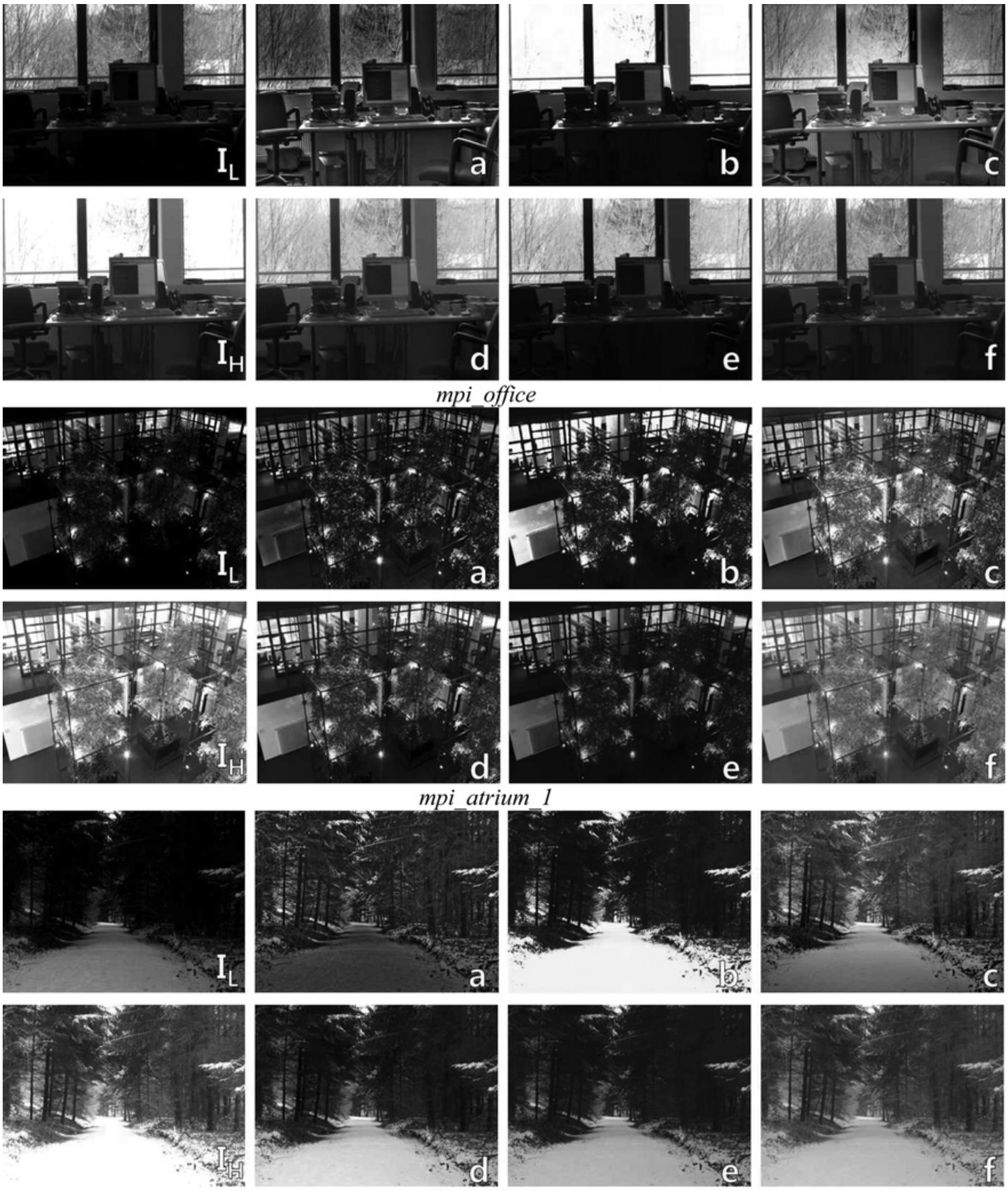

Fig. 10 *Additional comparisons of the results*

The left column is input, and right six images are results of
a Fattal
b Krawczyk
c Mertens
d Mantiuk
e Reinhard
f Proposed

Fig. 10 shows the additional results of comparisons. Since each image has six results of different algorithms, showing all images at once is not practical because of limited space. Therefore we only demonstrate mpi_office, mpi_atrium_1 and forest_path images in this paper.

To objectively evaluate the performances of the algorithms, we carried out performance assessment using HDR-VDP2 proposed by Mantiuk *et al.* in 2011 [29]. The goal of this metric is to perceptually linearise the differences between original and generated images so that the magnitude of distortion corresponds to visibility.

The test results are demonstrated in Table 2. The numerical values in the table are predicted mean opinion (MOS) where higher score means higher visual quality. Although the performances of conventional algorithms depend on the properties of test images, the proposed system shows stable and reliable results. Although the proposed algorithm is not ranked the highest in some images, the deficit is small.

doi: 10.1049/iet-ipr.2012.0614

Table 2 Results of objective quality assessment (predicted MOS)

Test image	Fattal	Krawczyk	Mertens	Mantiuk	Reinhard	Proposed
bristolb	42.3304	39.9851	49.9726	50.8560	46.3572	48.5475
crowfoot	40.3690	38.5353	56.1322	52.3816	45.5012	56.8019
oaks	39.1662	37.6295	46.0742	37.1183	37.3698	47.5341
tahoe1	33.0130	31.6127	36.7107	38.7137	36.4856	42.3622
clockbui	35.8344	25.9374	28.0123	33.7731	37.5946	43.8491
cornellbox	40.2365	28.2286	37.1308	44.2388	46.2619	44.8753
forest_path	39.5635	26.2078	36.8605	38.9511	42.0696	54.3236
wreathbu	29.5184	25.1278	24.6304	20.8994	43.2991	38.4862
mpi_atrium_1	36.7680	22.5142	35.8331	33.3559	34.6483	51.2068
mpi_atrium_3	34.2463	25.7163	36.5917	37.9166	39.1768	54.1262
mpi_office	30.4818	26.3085	31.7468	42.1761	34.2440	47.3356
nancy_church1	41.1308	35.9137	46.7799	48.0340	50.5980	55.6248
nancy_church2	32.8910	30.6465	37.8534	39.3210	55.0019	51.2351
nancy_church3	36.2526	26.1955	35.9851	34.1162	41.2974	52.2524
rosette	45.9246	43.7334	51.5579	48.5431	49.8788	54.6399
seymour_park	33.9708	30.0670	31.6821	34.1723	37.5549	50.2861
sunrendering	53.8374	58.7357	63.8519	65.3691	70.2631	81.2672
vinesunset	52.1495	30.7488	42.0351	44.0778	40.2243	51.6706
groveC	44.9451	33.8804	40.4261	43.7578	51.7301	52.1861
tinterna	33.6177	21.5131	30.8206	31.4535	28.0914	41.0550
average	38.8124	31.9619	40.0344	40.9613	43.3824	50.9833

Other than these, the proposed algorithm was given the highest rating in every dataset.

5 Conclusion

In this paper, we have proposed the algorithm to generate a low-bit depth-HDR image by blending two LDR images. In order to preserve the global intensity order and blend two image naturally, we adopted various techniques including cost aggregating, luminance adjusting and CG-based blending. From the experiments, results confirmed that the proposed algorithm generates more natural and vivid results than the state-of-the-art algorithms. In addition, the proposed algorithm achieved the highest score in objective evaluation. Hence, this technique is expected to be widely applied to various capturing and editing tools.

6 Acknowledgment

This work was supported by the National Research Foundation of Korea (NRF) grant funded by the Korea government (MEST) (grant no. 2012-0009228).

7 References

1 Mingli, S., Dacheng, T., Chun, C., Jiajun, B., Jiebo, L., Chengqi, Z.: ‘Probabilistic exposure fusion’, *IEEE Trans. Image Process.*, 2012, **21**, (1), pp. 341–357
2 Vonikakis, V., Andreadis, I., Gasteratos, A.: ‘Fast centre-surround contrast modification’, *IET Image Process.*, 2008, **2**, (1), pp. 19–34
3 Jha, R.K., Biswas, P.K., Chatterji, B.N.: ‘Contrast enhancement of dark images using stochastic resonance’, *IET Image Process.*, 2012, **6**, (3), pp. 230–237
4 Wang, C., Peng, J., Ye, Z.: ‘Flattest histogram specification with accurate brightness preservation’, *IET Image Process.*, 2008, **2**, (5), pp. 249–262
5 DiCarlo, J., Wandell, B.: ‘Rendering high dynamic range images’. The SPIE Electronic Imaging Conf., 2000
6 Mannami, H., Sagawa, R., Mukaigawa, Y., Echigo, T., Yagi, Y.: ‘High dynamic range camera using reflective liquid crystal’. IEEE Int. Conf. Computer Vision, 2007
7 Pardo, A., Sapiro, G.: ‘Visualization of high dynamic range images’, *IEEE Trans. Image Process.*, 2003, **12**, (6), pp. 639–647
8 Kim, Y.T.: ‘Contrast enhancement using brightness preserving bi-histogram equalization’, *IEEE Trans. Consum. Electron.*, 1997, **43**, (1), pp. 1–8
9 Menotti, D., Najman, L., Facon, J., de Araujo, A.A.: ‘Multi-histogram equalization methods for contrast enhancement and brightness preserving’, *IEEE Trans. Consum. Electron.*, 2007, **53**, (3), pp. 1186–1194
10 Im, J., Jeon, J., Hayes, M.H., Paik, J.: ‘Single image-based ghost-free high hynamic range imaging using local histogram stretching and spatially-adaptive denoising’, *IEEE Trans. Consum. Electron.*, 2011, **57**, (4), pp. 1478–1484
11 Tsai, C.-M., Yeh, Z.-M.: ‘Contrast enhancement by automatic and parameter-free piecewise linear transformation for color images’, *IEEE Trans. Consum. Electron.*, 2008, **54**, (2), pp. 213–219
12 Tumblin, J., Rushmeier, H.: ‘Tone Reproduction for realistic images’, *IEEE Comput. Graph. Appl.*, 1993, **13**, (6), pp. 42–48
13 Larson, G.W., Rushmeier, H., Piatko, C.: ‘A visibility matching tone reproduction operator for high dynamic range scenes’, *IEEE Trans. Vis. Comput. Graph.*, 1997, **3**, (4), pp. 291–306
14 Drago, F., Myszkowski, K., Annen, T., Chiba, N.: ‘Adaptive logarithmic mapping for displaying high contrast scenes’. EUROGRAPHIC, Wiley Online Library, 2003
15 Fattal, R., Lischinski, D., Werman, M.: ‘Gradient domain high dynamic range compression’, *ACM Trans. Graph.*, 2002, **21**, (3), pp. 249–256
16 Reinhard, E., Devlin, K.: ‘Dynamic range reduction inspired by photoreceptor physiology’, *IEEE Trans. Vis. Comput. Graph.*, 2005, **11**, (1), pp. 13–24
17 Mantiuk, R., Daly, S., Kerofsky, L.: ‘Display adaptive tone mapping’, *ACM Trans. Graph.*, 2008, **27**, (3), pp. 68
18 Krawczyk, G., Myszkowski, K., Seidel, H.P.: ‘Lightness perception in tone reproduction for high dynamic range images’. Computer Graphics Forum, Wiley Online Library, 2005
19 Gelfand, N., Adams, A., Park, S.H., Pulli, K.: ‘Multi-exposure imaging on mobile devices’. Int. Conf. Multimedia, 2010
20 Mertens, T., Kautz, J., Van Reeth, F.: ‘Exposure fusion’. Pacific Conf. Computer Graphics and Applications, 2007
21 Jinno, T., Okuda, M.: ‘Multiple exposure fusion for high dynamic range image acquisition’, *IEEE Trans. Image Process.*, 2012, **21**, (1), pp. 358–365
22 Goshtasby, A.A.: ‘Fusion of multi-exposure images’, *Image Vis. Comput.*, 2005, **23**, (6), pp. 611–618
23 Ning, S., Mansour, H., Ward, R.: ‘HDR image construction from multi-exposed stereo LDR images’. IEEE Int. Conf. Image Processing, 2010
24 Sharma, M., Chaudhury, S., Lall, B.: ‘Parameterized variety for multi-view multi-exposure image synthesis and high dynamic range stereo reconstruction’. 3DTV-Conf. The True Vision – Capture, Transmission and Display of 3D Video (3DTV-CON), 2012
25 Li, S.Z.: ‘Markov random field modeling in image analysis’ (Springer, 2009)
26 Felzenszwalb, P.F., Huttenlocher, D.P.: ‘Efficient belief propagation for early vision’, *Int. J. Comput. Vis.*, 2006, **70**, (1), pp. 41–54
27 Gill, P.E., Murray, W.: ‘Algorithms for the solution of the nonlinear least-squares problem’, *SIAM J. Numer. Anal.*, 1978, **15**, (5), pp. 977–992
28 Qingxiong, Y., Kar-Han, T., Ahuja, N.: ‘Real-time O(1) bilateral filtering’. IEEE Conf. Computer Vision and Pattern Recognition, 2009
29 Mantiuk, R., Kim, K.J., Rempel, A.G., Heidrich, W.: ‘HDR-Vdp-2: a calibrated visual metric for visibility and quality predictions in all luminance conditions’, *ACM Trans. Graph.*, 2011, **30**, (4), p. 40